Chinese Chemical Letters 37 (2026) 111552

Contents lists available at ScienceDirect

Chinese Chemical Letters

journal homepage: www.elsevier.com/locate/cclet

Fluorescence excitation strategies driven by different energy sources: Mechanism, molecular/materials design, and cross-applications

Jingwen Zheng[a,d,1], Yubo Tan[a,1], Dazhuang Xu[c,*], Gang Liu[c,*], Zhixiang Lu[b,d,*]

[a] State Key Laboratory of Molecular Vaccinology and Molecular Diagnostics, State Key Laboratory of Vaccines for Infectious Diseases, Center for Molecular Imaging and Translational Medicine, Xiang An Biomedicine Laboratory, School of Life Sciences, Xiamen University, Xiamen 361102, China
[b] State Key Laboratory of Vaccines for Infectious Diseases, Fujian Provincial Key Laboratory of Innovative Drug Target Research, Xiang An Biomedicine Laboratory, School of Pharmaceutical Sciences, Xiamen University, Xiamen 361102, China
[c] State Key Laboratory of Molecular Vaccinology and Molecular Diagnostics, State Key Laboratory of Vaccines for Infectious Diseases, Center for Molecular Imaging and Translational Medicine, Xiang An Biomedicine Laboratory, School of Public Health, Xiamen University, Xiamen 361102, China
[d] Sichuan Research Institute of Xiamen University, Chengdu 610000, China

ARTICLE INFO

Article history:
Received 28 March 2025
Revised 3 July 2025
Accepted 7 July 2025
Available online 7 July 2025

Keywords:
Fluorescence imaging
Fluorescence excitation strategies
Mechanism
Classification
Cross-applications

ABSTRACT

As a technique with high sensitivity and resolution, fluorescence imaging is widely used in biomedical research, disease diagnosis and environmental monitoring, *etc*. Traditional fluorescence imaging mostly relies on photoexcitation paradigms, but with the deepening of multidisciplinary cross research, fluorescence excitation strategies based on multiple energy sources have gradually become an emerging frontier. These innovative strategies achieve diversified excitation of fluorescent probes by using multiple external stimuli, such as electric energy, magnetic energy, chemical energy, electromagnetic radiation, optical energy and mechanical energy, providing more flexible choices for different application scenarios, which not only broaden the application scope of fluorescence technology but also provide a new way of thinking for the design of highly efficient and tunable fluorescence systems. To track the latest advancements in fluorescence excitation techniques, this review systematically summarizes the recent multiple energy sources, focusing on their mechanisms, design principles, application prospects and challenges. By synthesizing recent research progress, this work aims to highlight emerging excitation strategies and offer valuable insights for developing next-generation fluorescent probes and broadening the technological applications of fluorescence-based systems.

© 2026 Published by Elsevier B.V. on behalf of Chinese Chemical Society and Institute of Materia Medica, Chinese Academy of Medical Sciences.

1. Introduction

In 1888, the term "luminescence" was first introduced by the German physicist Eilhardt Wiedemann [1]. It was proposed that the light emitted by incandescent lamps and that produced by fluorescence represent fundamentally different phenomena. To distinguish light generated by heat (incandescence) from light emitted without significant heat (cold light), the term "luminescence" was coined to describe the latter. This distinction helped clarify the underlying mechanisms of light emission. Luminescence was subsequently classified into six types based on the excitation mechanism: triboluminescence, chemiluminescence (CL), photoluminescence (PL), thermoluminescence, electroluminescence (EL), and bioluminescence (BL) [2].

Recently, fluorescence technology has emerged as a valuable tool across various fields, due to its distinct advantages and extensive applications [3–7]. The use of light energy to stimulate fluorescence is the earliest recorded method and remains the most common and widely applied approach [8]. Driven by technological advancements, light-induced fluorescence has found extensive application across multiple domains, including oncology surgical navigation and intelligent phototherapy nanoprobes. These developments are broadening the horizons for the clinical application of light-induced fluorescence, paving the way for more accurate and convenient diagnostic and therapeutic approaches.

In addition to traditional light excitation, fluorescence can be induced by mechanical, X-ray, chemical energy, EL, and magnetoluminescence. Ultrasound enables deep tissue penetration to induce local fluorescence, making it essential in medical applications [9]. Electromagnetic radiation (X-ray/γ-ray)-induced fluores-

* Corresponding authors.
E-mail addresses: dazhuangxu1994@163.com (D. Xu), gangliu.cmitm@xmu.edu.cn (G. Liu), zhixiangl@xmu.edu.cn (Z. Lu).
[1] These authors contributed equally to this work.

https://doi.org/10.1016/j.cclet.2025.111552
1001-8417/© 2026 Published by Elsevier B.V. on behalf of Chinese Chemical Society and Institute of Materia Medica, Chinese Academy of Medical Sciences.



Scheme 1. Schematic illustration of fluorescence excitation strategies induced by different energy sources. CROSS: CROSS applications.

cence offers high sensitivity for subcellular imaging, alloy element analysis, drug trace detection, and archaeological sample analysis [10–12]. Endogenous light-induced fluorescence avoids photobleaching and scattering without external light sources. For example, luminol-based chemiluminescent probes detect cellular reactive oxygen species (ROS) for oxidative stress/apoptosis analysis [13] and assist in crime scene trace evidence detection [14]. EL is key in organic light-emitting diode (OLED) displays for smartphones/TVs due to high contrast and flexibility [15–18], and in energy-efficient lighting like flexible EL panels. Emerging magnetoluminescence applications include tumor imaging, drug delivery, and thermotherapy *via* magnetofluorescent nanostructures [19,20], opening new technological frontiers.

In each subsection of this review, we discuss the excitation of fluorescent molecules/materials under the stimulation of different energy sources, explore the underlying excitation mechanisms, and highlight the advantages of these materials through recent practical applications. Finally, we also clarify the current challenges in this field's excitation strategies and the potential for future development. Our aim is to inspire researchers to make novel discoveries, foster the growth of multimodal imaging, and broaden application possibilities by integrating diverse fluorescence excitation modes and strategies. The flexible adaptation in accordance with application scenario will reduce technical costs and enhance performance to achieve optimal application outcomes (Scheme 1).

2. Fluorescence excitation driven by different energy sources

2.1. Light-excited fluorescence

Photoluminescence involves photon absorption, excited-state transition, and radiative relaxation emitting fluorescence. Laser-induced fluorescence imaging (LIF) has evolved from single-photon excitation [21,22] and confocal microscopy [23] to multiphoton, near-infrared (NIR) [24], and super-resolution techniques [25], with NIR-II probes [26] and multimodal integration advancing deep tissue imaging [27–29].

Single-photon probes combined with single-photon microscopy are widely used for targeting various biomolecules and organelles [30]. However single-photon excitation fluorescence (SPEF) is primarily suitable for imaging superficial tissues or single-cell layers, and often exhibits high background signals and low spatial resolution. Recently, two-photon fluorescence imaging has received special attention due to its lower photobleaching, autofluorescence, deeper tissue penetration ability and higher three-dimensional resolution. Two-photon absorption (TPA) describes a nonlinear optical process in which a molecule simultaneously absorbs two photons under specific conditions, transitioning from a lower energy state to a higher one. When the excited electron relaxes back to the ground state, the molecule emits fluorescence, a phenomenon termed two-photon excitation fluorescence (TPEF) [31]. Classical TPA relies on femtosecond pulsed lasers with extremely high power densities for excitation [32], making the development of materials with large TPA cross-sections (δ) or low-power triggering systems crucial [33–35]. Meng *et al.* constructed MOFs (Zn-BTPPA and Cd_3-BTPPA) that showed enhanced TPEF under 780 nm excitation, with TPA δ 4.9 and 5.2 times higher than reported dinuclear MOFs, offering new design insights (Fig. 1A) [36]. However, MOFs have complex synthesis, high preparation costs, and poor batch reproducibility [37].

As research advances, scientists are exploring the integration of TPA technology with fluorescent probes [38]. These probes utilize the properties of TPA materials to effectively reduce autofluorescence interference, with wide applications in the detection or imaging of cations (*e.g.*, Zn^{2+}, Pd^{2+}), anions (*e.g.*, $ONOO^-$, ClO^-), biological macromolecules, cells, and subcellular localization [33]. Zhang *et al.* designed two novel two-photon fluorescent probes, P1 and P2, featuring a D-π-A structure by connecting benzothiazole and benzimidazole to *N*,*N*-diphenylaniline *via* pyridine vinyl (Fig. 1B) [39]. Compared to traditional fluorescent probes, these exhibit significantly higher TPA δ, penetrate cell membranes, specifically localize in mitochondria, and show excellent fluorescence imaging capabilities in zebrafish *in vivo* experiments.

When designing TPA probes for biological systems, increasing the TPA δ of TP fluorophores is not the only consideration; fluorescence quantum yield and absorption wavelength are also essential. Biological applications often require additional properties like water solubility, imaging brightness, and duration. Fu *et al.* combined silica nanodots with the organic fluorophore ANPA-N_3, enhancing probe water solubility through hydrophilic surface modification of silicon nanodots (SiND) [40]. The probe enables highly sensitive hydrogen sulfide (H_2S) detection in fully aqueous environments and is successfully applied to two-photon imaging of living cells and onion tissues (Fig. 1C). Chen *et al.* enhance TPA efficiency by introducing a rigid styryl conjugated unit to boost intramolecular charge transfer, improve water solubility using pyridinium positively-charged groups, and achieve tumor-specific enrichment through modular targeting ligand modification [41].

Although TPA probes enable fluorescence imaging in cells and live animals, they rely on fluorescence intensity as the main signal metric, lacking the ability to provide functional information. Two-photon fluorescence lifetime imaging microscopy (TP-FLIM) was developed to address this, integrating two-photon excitation with FLIM [42]. However, most reported TP-FLIM probes are exclusively targeted to DNA or RNA. Guo *et al.* synthesized fluorine-nitrogen co-doped carbon dots (F-NCDs) [43]. As TP-FLIM probes, F-NCDs can target nuclear nucleic acids through electrostatic adsorption. They enable quantitative multicolor imaging of DNA/RNA in all stages of mitosis in onion root tip cells and in zebrafish embryonic and eye tissues, with an imaging depth of up to 70 μm. The probes can distinguish between retinal cells and lens cells (Fig. 1D), and retain over 80 % of their fluorescence intensity after 30 min of continuous excitation. This provides a highly stable tool for dynamically resolving the distribution and metabolism of genetic material .

The potential of two-photon excitation extends beyond imaging, as its application in photodynamic therapy (PDT) is increasingly attracting attention [26]. Bondon *et al.* synthesized a multifunctional periodic mesoporous organosilica nanoparticle platform (PMO NPs) (Fig. 1E), enhancing biocompatibility and tumor targeting through surface PEGylation and mannose (MAN) ligand modification. Pho-

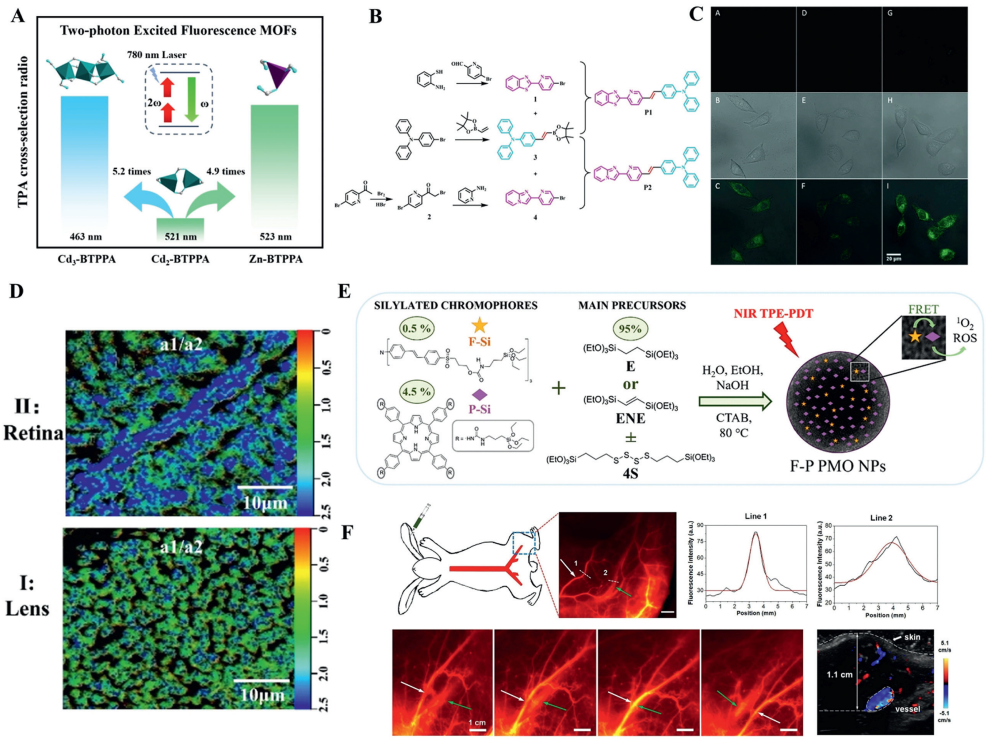


Fig. 1. (A) Scheme for modulation of inorganic nodes to enhance TPEF in metal-organic framework single crystals. Reproduced with permission [36]. Copyright 2024, American Chemical Society. (B) Scheme to illustrate the molecules and synthesis route of probes P1 and P2. Reproduced with permission [39]. Copyright 2024, Elsevier. (C) Schematic illustration of two-photon confocal microscopy images of MCF-7 cells incubated with SiND-ANPA-N_3. Reproduced with permission [40]. Copyright 2013, Royal Society of Chemistry. (D) Scheme to illustrate the TP-FLIM imaging of nuclei and intranuclear DNA/RNA in zebrafish eyes. Reproduced with permission [43]. Copyright 2025, American Chemical Society. (E) Schematic illustration of synthesis conditions of fluorophore-porphyrin (F-P) PMO NPs. Reproduced with permission [44]. Copyright 2024, Elsevier. (F) Scheme for NIR-II fluorescence imaging of the vasculature in the rabbit. Reproduced with permission [52]. Copyright 2021, Elsevier.

tophysical studies reveal that F-P PMO NPs exhibit fluorescence resonance energy transfer (FRET) efficiency as high as 83 %–93 %, with a TPA cross-section of 205 gigamolar (GM) in the 700–850 nm range. Under NIR excitation, their ROS generation efficiency significantly outperforms single-photon excitation [44]. However, conventional TPEF materials still face limitations in biomedical applications such as poor biocompatibility, insufficient photostability, and limited tumor targeting.

In recent years, NIR-II fluorescence imaging has improved spatio-temporal resolution and penetration depth [45–47]. Its targeting strategies are divided into active and passive targeting. The latter relies on the enhanced permeability and retention (EPR) effect but has low efficiency, while the former achieves precise enrichment through specific binding of ligands, which is suitable for the identification of avascular tumors [48]. Li *et al.* developed dual-targeting DT-PNPs for glioblastoma, achieving 92 % tumor inhibition and 32-day median survival *via* 808 nm laser triggering [49]. However, NIR-II imaging lacks comprehensive anatomical information, driving the need for multimodal imaging [50]. Sun *et al.* used a probe combining small-molecule dyes with melanin nanoparticles to achieve NIR-II fluorescence/PA dual-modal imaging of laryngeal cancer [51]. Li *et al.* first validated the feasibility of NIR-II angiography in large animals (rabbits) (Fig. 1F) [52].

Photoluminescent materials show mature applications but face scenario-specific requirements [53]. Biomedical imaging prioritizes penetration and safety, environmental monitoring focuses on anti-interference, and display technologies seek excitation efficiency. Current NIR-II multimodal imaging studies have potential but remain preliminary [54]. Future research should develop novel multimodal probes by integrating metal-organic frameworks or up-conversion nanoparticles with NIR-II dyes for simultaneous fluorescence, photoacoustic, and magnetic resonance imaging. Smart probes responsive to physiological markers will enable dynamic disease monitoring for personalized medicine. Despite a solid foundation, continuous innovation in probe design and clinical translation is needed to unleash NIR-II multimodal imaging's full potential.

2.2. Mechanically induced fluorescence

In recent years, flexible sensors in AI skin, wearables, and smart healthcare have thrived due to flexibility and adaptability. For example, smart wristbands convert mechanical stress (pinching/bending) into visual signals like green light spots for function switching [55]. Mechanoluminescent (ML) materials enable this conversion, with narrow-sense ML from friction/impact and modern strategies *via* piezoelectric/catalytic energy transfer. Wang *et al.* tuned CdS nanocrystals' luminescence *via* pressure-ligand engineering, shifting emission from orange to blue-violet under high pressure (Fig. 2A) [56], but sulfide materials lack environmental stability [57]. Inorganic ML materials (*e.g.*, $SrAl_2O_4:Eu^{2+}$) incur high costs [58], while organic ML suffers from luminescent non-uniformity [59]. To address this, Xie *et al.* designed and synthesized a series of flexible amorphous organic small molecules (BPON-1 to BPON-5) (Fig. 2B) [60]. With low glass transition temperatures (56–78.5 °C), these molecules can be regenerated *via* thermal annealing, thus promoting the development of amorphous ML materials.

Ultrasound-based imaging is a core clinical tool for real-time, safe, and low-cost tissue imaging. Acoustic luminescence was discovered in 1934 but has limited utility [61,62]. In 1880, the Curie brothers discovered the piezoelectric effect, where mechanical stress deforms crystals to generate surface charges, converting mechanical to electrical energy [63–66]. A novel ultrasound-excited fluorescence strategy converts mechanical energy to elec-

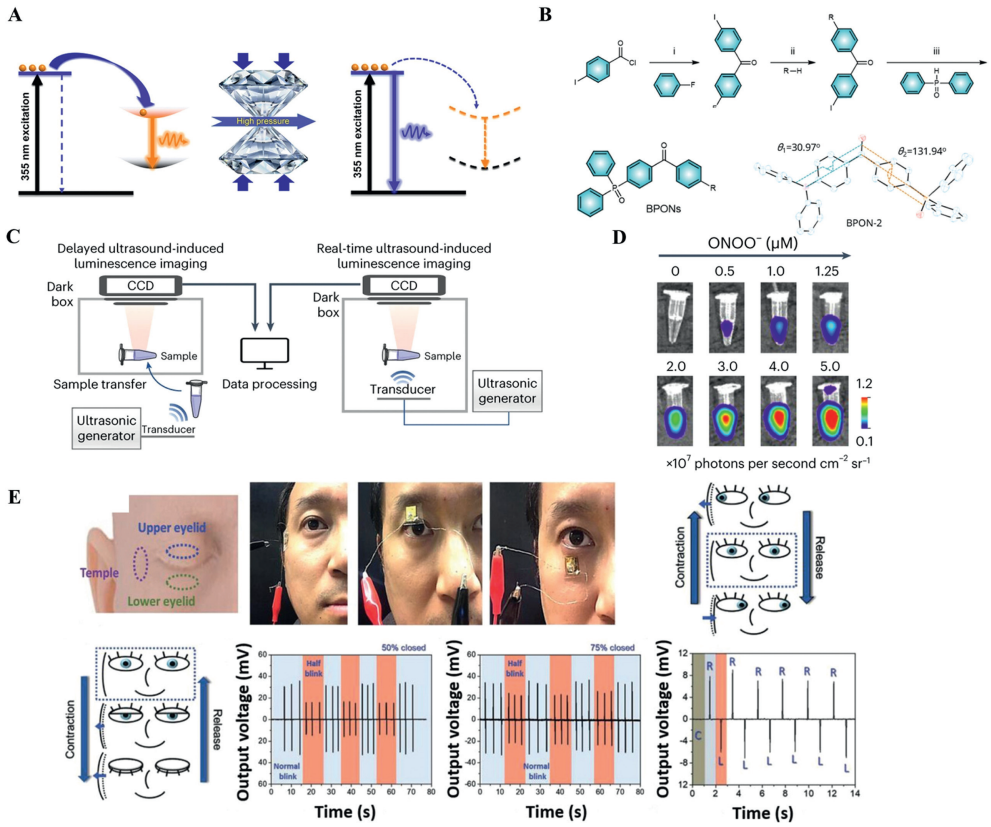


Fig. 2. (A) Illustration of the energy level changes upon compression. Reproduced with permission [56]. Copyright 2025, John Wiley and Sons. (B) Scheme for the design strategy and synthesis of BPONs. Reproduced with permission [60]. Copyright 2025, American Chemical Society. (C) Schematic illustration of experimental setup for delayed ultrasound-induced luminescence imaging (left) and real-time ultrasound-induced luminescence imaging (right). (D) Scheme for delayed ultrasound-induced luminescence imaging of TD@IR780 NPs. Reproduced with permission [68]. Copyright 2024, Springer Nature. (E) Schematic diagram of eye movement measurement. Reproduced with permission [63]. Copyright 2022, John Wiley and Sons.

trical *via* piezoelectric materials, driving ROS generation and CL [67]. Recently, Wang *et al.* developed a technique to generate ultrasound-induced molecular luminescence from organic nanoparticles *via* nanoscale piezoelectric effects and piezoelectric catalysis, first completing *in vivo* fluorescence imaging with ultrasound [68]. They investigated various ultrasound-responsive luminescents by incorporating them into polymer nanoparticles to identify the most effective ultrasound-responsive luminescence in two imaging models: real-time ultrasound-induced luminescence imaging and delayed ultrasound-induced luminescence imaging (Fig. 2C). They specifically used tri-anthracene derivative-based nanoparticles (TD NPs) (Fig. 2D). Compared with acoustic luminescence in water, TD NPs exhibit a 2000-fold increase in luminous intensity, a 10-fold increase in signal-to-noise ratio (SNR) compared to fluorescence imaging, a spatial resolution of 1.46 mm, a tissue penetration depth of 2.2 cm, and a half-life of up to 3 min. Undoubtedly, this technology demonstrates great potential for further development and application. Delayed ultrasound-induced luminescence (acoustic afterglow imaging) offers low autofluorescence. Xu *et al.* designed sonoafterglow nanoparticles (SNAP) with two-step energy conversion, and sonoafterglow imaging and immunotherapeutic functionality (SCAN) nanoparticles combining afterglow imaging and immunotherapy. SCAN releases immunomodulators in tumor microenvironments, showing potential for cancer treatment and precision medicine [69].

In summary, ML finds broad applications in modern technology but faces bottlenecks in signal efficiency and practical implementation. For ML dominated by the concept of ML, the excitation efficiency is closely correlated with the magnitude of mechanical stress, with overall low material preparation costs and good economic feasibility. It is widely used in detecting minute physiological signals and human motion, for example, GaN thin film/PDMS flexible sensors for eye movement and fatigue monitoring, and PVDF/BTO nanofiber membrane sensors that distinguish exercise modes *via* voltage output variations with angle (Fig. 2E) [63]. Nevertheless, such ML suffers from shallow penetration depth, with imaging sensitivity limited by material luminescence efficiency that highly depends on molecular ordering; pure materials often exhibit weak luminescence, and while amorphous states address flexibility, their quantum yields are generally lower than crystalline or photoluminescent materials. Luminescence degradation is evident after repeated mechanical actions due to defect saturation. In contrast, ultrasound-excited nanoparticles *via* two-step energy conversion significantly enhance SNR, penetration depth, and resolution compared to traditional fluorescence imaging, making them suitable for deep clinical scenarios like tumor immunotherapy monitoring. Targeted modification can improve lesion recognition, but challenges include high equipment costs, complex nanoparticle synthesis, and limited research, though their superior biocompatibility offers exciting prospects for precise deep-tumor imaging and blood-brain barrier intervention.

2.3. Radiant energy-excited fluorescence

2.3.1. X-ray-induced fluorescence (XRF)

X-rays are electromagnetic waves with a wavelength of 0.01–10 nm with high energy and penetrating power [70]. XRF, as a rapid, portable, and non-destructive analytical technique, is widely applied in materials science, environmental science, geology, industrial production, and other fields. By using X-rays to excite

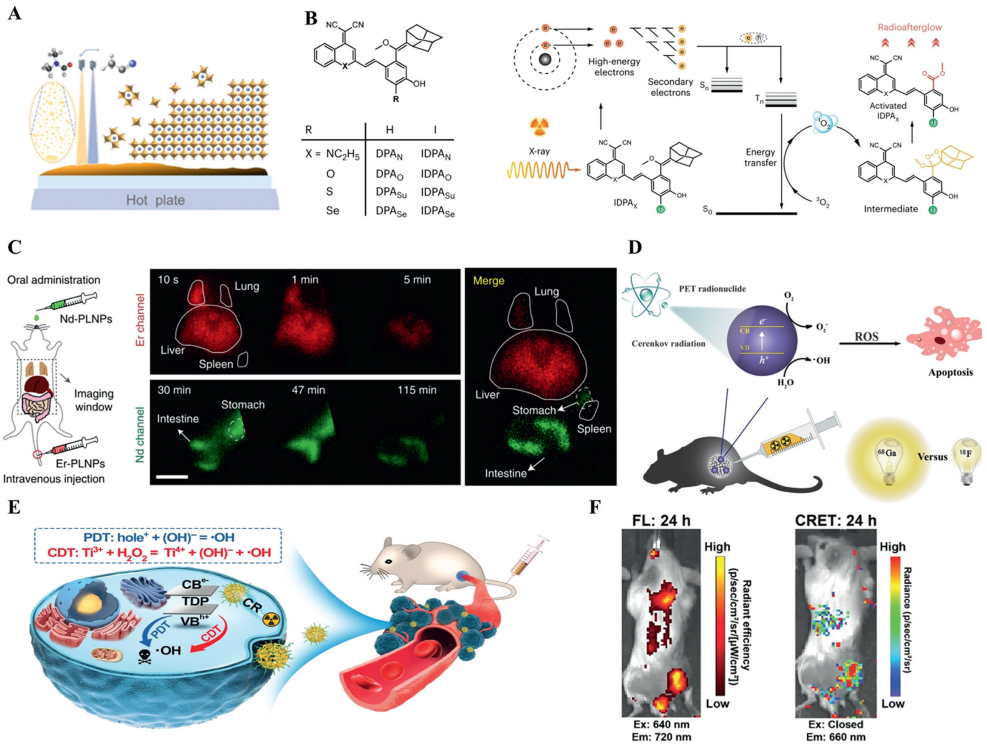


Fig. 3. (A) Schematic illustration of spray-coating process. Reproduced with permission [75]. Copyright 2023, Elsevier B.V. (B) Chemical structures of DPAs and IDPAs and schematic of the proposed radio afterglow mechanism. Reproduced with permission [76]. Copyright 2023, Springer Nature. (C) Scheme for the dual-channel *in vivo* PL imaging of organs in a living mouse. Reproduced with permission [78]. Copyright 2021, Springer Nature. (D) Scheme for the mechanism of the ROS generation of D-TiO_2NPs. Reproduced with permission [83]. Copyright 2018, American Chemical Society. (E) Schematic diagram of TDP NPs for CRICT against tumors. Reproduced with permission [84]. Copyright 2021, American Chemical Society. (F) Scheme for the FL and CRET images of ^{89}Zr-DFO-MEP5 within the tumor. Reproduced with permission [93]. Copyright 2023, John Wiley and Sons.

inner-shell electrons in sample atoms, it triggers the emission of characteristic fluorescent X-rays [71,72].

On this basis, X-ray imaging can be achieved through indirect or direct imaging [73]. Here, we focus on X-ray-induced fluorescence, an indirect imaging technique using X-ray luminescent materials. X-ray-induced fluorescence materials refer to substances that generate characteristic fluorescent signals under X-ray excitation, showing great potential in radiation detection, biological imaging, and cancer therapy. These include inorganic scintillator materials (*e.g.*, CsI), rare-earth-doped fluorescent materials (*e.g.*, Gd_2O_2S:Tb), semiconductor fluorescent materials, and rare-earth nanoparticles. However, traditional X-ray detection materials face several challenges in practical applications. For instance, $Bi_4Ge_3O_{12}$ and CsI:Ti scintillators require high synthesis temperatures and are prone to moisture issues. While organic molecules and metal halide chalcogenides show high-intensity radioluminescence and efficient X-ray absorption, they often suffer from poor stability, susceptibility to decomposition, and the necessity of a thick active layer to fully absorb X-ray photons [74]. However, the traditional spin-coating technique can only prepare thin films, and the traditional spray-coating technique is difficult to obtain high-quality thick chalcogenide films. Jia *et al.* proposed an anti-solvent-assisted spray coating technique, which is able to prepare thick films with small surface roughness and adjustable thickness on various substrates (Fig. 3A) [75]. They further prepared X-ray detectors based on spray-coated thick chalcogenide films, and the results showed that the optimized X-ray detectors exhibited sensitivities as high as 3370.8 μC Gy^{-1} cm^{-2} demonstrating their great potential for X-ray detection applications.

X-ray-activated nanoscale materials offer tunable NIR-II luminescence. And X-ray-induced radioluminescence afterglow imaging (RAI) addresses tissue penetration limitations. Huang *et al.*'s organic luminophore (IDPA) (Fig. 3B) generates NIR afterglow and $^1O_2$ for cancer theranostics, showing 25 times brighter *in vivo* afterglow than inorganic nanophosphors [76]. Zhang *et al.* developed $Cs_2Na_{0.9}Ag_{0.1}LuCl_6$:$Dy^{3+}$ long-afterglow crystals, preparing flexible X-ray detectors with >2-h afterglow [77]. Pei *et al.* reported lanthanide-doped PL nanoparticles (Ln-PLNPs) with 72-h persistent NIR-II emission for *in vivo* imaging (Fig. 3C) [78]. Chen *et al.* designed $LiGa_5O_8$:Cr-based nanoscintillators for X-ray-guided tumor therapy [79]. Challenges include nanoparticle size, rare-earth toxicity, low energy conversion (1 %–5 %), and targeting limitations.

In summary, the application of X-ray-induced fluorescence technology requires balancing performance optimization, biomedical safety, and economic feasibility. For example, in the medical field, materials like CsI and Gd_2O_2S are preferred for their sensitivity and large-area imaging capabilities. Inorganic rare-earth materials are suitable for high-resolution imaging but carry metal toxicity risks. Metal halide perovskites (*e.g.*, $CsPbBr_3$) offer a fluorescence quantum yield exceeding 90 % and low preparation costs, but their lead toxicity restricts clinical application. Organic smart probes exhibit excellent biocompatibility and enable molecular-level imaging, yet their low X-ray absorption efficiency necessitates the introduction of iodinated groups to enhance the photoelectric effect. Future trends are likely to focus on multifunctional integration and biocompatibility optimization, promoting the design of intelligent probes, novel nanoparticles, and semiconductor materials to advance precision medicine and improve diagnostic specificity.

2.3.2. Cerenkov radiation (CR)-induced fluorescence

CR refers to the electromagnetic radiation generated when high-energy charged particles from radioactive decay travel through a medium faster than the speed of light in that medium, causing molecular polarization and subsequent relaxation [80]. The

intensity depends on particle velocity and the medium's refractive index, requiring no exogenous probes. Cherenkov luminescence imaging (CLI) has emerged as a novel imaging technology by directly converting clinically routine radioactive tracers into optical signals, significantly expanding the repertoire of optical probes in biomedicine [81]. Cherenkov luminescence has currently found wide applications in various fields, including labeled biomolecule detection, medical imaging with radionuclides, nuclear reactors, astrophysical experiments, and particle physics research. But the short wavelength of Cherenkov luminescence limits its imaging depth due to strong absorption by tissues, typically restricting its use to superficial or small-animal models and necessitating more suitable endoscopic materials.

In 2015, Kotagiri *et al*. reported an oxygen-independent activation of TiO_2-based nano-photosensitizers (PS) *via* radionuclide-induced CR, advancing depth-independent CR-mediated PDT (CRIT) for cancer [82]. However, ^{18}F's low CR productivity requires 10–30 times higher doses. Duan *et al*. first doped ^{68}Ga into dextran-modified TiO_2 NPs (D-TiO_2 NPs) for CR-PDT (Fig. 3D) [83]. ^{68}Ga-BSA showed stronger 4T1 cell growth inhibition and DNA damage than ^{18}F-FDG, with D-TiO_2 NP/^{68}Ga-BSA suppressing tumor growth in mice. Current CRIT type I PS are TiO_2-based but face targeting issues. Li *et al*. developed NH_2-$Ti_{32}O_{16}$ nanocluster PS (TDPs) (Fig. 3E) [84]. The introduction of dopamine (DA) ligands can improve tumor-targeting behavior through binding affinity to DA receptors on cancer cells. However, recent studies have revealed that strategies coupling radionuclides with PS lead to severe side effects, including pharmacokinetic mismatch. Qian *et al*. developed tumor-targeting nanoparticles named ^{131}I-EM@ALA. Wu *et al*. achieved safe and efficient CRIT through the synergistic action of pH-responsive PS nanocomposites (BCM) and a targeted CR delivery system (^{68}Ga-C2) [85]. *In vitro* experiments show this strategy achieves a 90 % tumor cell kill rate with low normal cell toxicity, while *in vivo* studies confirm significant tumor growth inhibition without obvious systemic toxicity [85].

Cherenkov-induced fluorescence (CIF) converts short-wavelength CR to long-wavelength light *via* fluorescent probes for deeper tissue penetration [86,87], using probes like quantum dots (QDs) and lanthanide nanomaterials [88–90]. Li *et al*.'s lanthanide NPs enhanced energy conversion by 7.72 times *via* gradient doping, achieving 8.1:1 tumor-to-background ratio and 2.5 cm penetration in prostate cancer (hemolysis <1.5 %) [91]. Hu *et al*.'s squaraine-sensitized UCNPs showed 97 times luminescence enhancement and 68 % energy transfer efficiency, with 1.8 cm penetration in mice (hemolysis <2 %) [92]. Rosenkrans *et al*. optimized PS-doped SPNs for near-100 % CR energy transfer, developing NIR QDs/^{89}Zr nanoplatforms to convert CR to NIR light (Fig. 3F).

Cherenkov luminescence imaging effectively utilizes the luminescence produced by radionuclide decay, so it could maximize the capabilities of existing positron emission tomography (PET)/single photon emission computed tomography (SPECT) probe devices. Future designs of biocompatible optical probes with large Stokes shifts are essential for enhancing the efficiency and safety of CRIT. Noted limitations include dependence on tissue oxygenation and low light penetration in tissues. In conclusion, the application of Cherenkov-induced fluorescence technology in different scenarios primarily requires adjustments based on probe performance. Enhancing excitation efficiency may exacerbate tissue scattering noise and reduce signal-to-noise ratio, while NIR fluorescent probes, though capable of deeper tissue penetration, have lower absorption δ for Cherenkov blue light and require radionuclide dose compensation, carrying radiation safety risks. Future research directions include developing more types of activatable probes, which are expected to advance the application of CIF technology in biomedical research and clinical diagnosis.

2.4. Endogenous energy-induced fluorescence

In 1948, after Theodor Förster proposed the equation to quantify the excitation transfer efficiency from energy donors to acceptors, technologies based on the resonance energy transfer (RET) mechanism became research hotspots in various fields. Depending on the energy donor, RET can be classified into FRET, phosphorescence resonance energy transfer (PRET), chemiluminescence resonance energy transfer (CRET), and bioluminescence resonance energy transfer (BRET) [94,95]. CRET technology emerged in 1967 as an energy transfer mechanism, in which a donor molecule is excited through a chemical reaction and then transfers energy to an acceptor molecule [96]. BRET, meanwhile, utilizes energy released from luciferase reactions to promote energy transfer between donor luminescent molecules and acceptor photosensitive molecules. Both CRET and BRET belong to the category of endogenously excited fluorescence. In 2021, Lou *et al*. quantitatively confirmed for the first time that the efficiency of charge RET is inversely proportional to the sixth power of the distance between the luminescent donor and tetraphenylethylene acceptor, indicating that CRET adheres to Förster's RET theory (Fig. 4A) [97]. "Endogenous" in CL and BL refers to internal energy generation *via* chemical/biological processes, eliminating external excitation. This avoids scattering interference, enabling low-noise, high-sensitivity detection for *in vivo* deep tissue and single-cell analysis. Applications include chemiluminescence immunoassay (CLIA) for tumor markers (fg/mL sensitivity), luminal reagent spraying for latent blood detection (10^6 dilution), and luciferase reporter genes for BL tomography in drug screening [98,99].

2.4.1. Chemically induced fluorescence

CL reactions are now widely used as a new tool *in vivo* bioimaging and therapeutics [100,101]. In the field of bioimaging, its unique property of not requiring external light source excitation allows it to avoid background fluorescence interference, making it particularly suitable for deep tissue imaging. Additionally, CLIA is widely used in clinical diagnostics for the detection of tumor markers, hormones, and other analytes [102]. Depending on the mechanism of chemical energy conversion, CL can generally be classified into direct CL and indirect CL [103,104]. Core materials include luminescent agents, fluorescent acceptors, catalysts, and nanomaterials [105]. Traditional luminol-based CL suffers from blue emission and shallow penetration, prompting innovations like Chen *et al*.'s NIR-II single-molecule probes (CLX3) [106]. Built on Schaap dioxetane, these fluoride-activated probes with DCMO units emit at 1060 nm, enabling 1.2 cm deep superoxide detection in liver injury models (Fig. 4B) with 13.5 signal-to-background ratio (SBR), outperforming traditional NIR fluorophores. Li *et al*. developed DTLum NPs, aggregation-induced emission (AIE)-type chemiluminescent probes linking luminol to donor-acceptor (D-A) structured diketopyrrolopyrrole [107]. Activated by singlet oxygen ($^1O_2$) under acidic conditions, DTLum NPs emit a strong NIR CL signal at 651 nm, combining AIE properties with deep tissue penetration (12.5 mm), significantly outperforming traditional fluorescence (<2.5 mm) (Fig. 4C). Tumor-targeting nanocolloids using luminol and Ce6 exploit CRET to generate $^1O_2$ in the TME (Fig. 4D), where H_2O_2 triggers $^1O_2$-mediated mRNA modification *via* furan oxidation [108]. This self-initiated gene therapy system covalently modifies mRNA without external light, monitored by fluorescence imaging, offering a novel RNA-based tumor therapy strategy.

The core advantages of CL lie in its independence from external light sources, deep tissue penetration capability, and multimodal integration potential, making it irreplaceable in high-sensitivity detection and dynamic imaging. However, traditional probes decays by over 90 % within minutes, failing to meet the needs of long-term dynamic imaging and suffering from insufficient brightness.

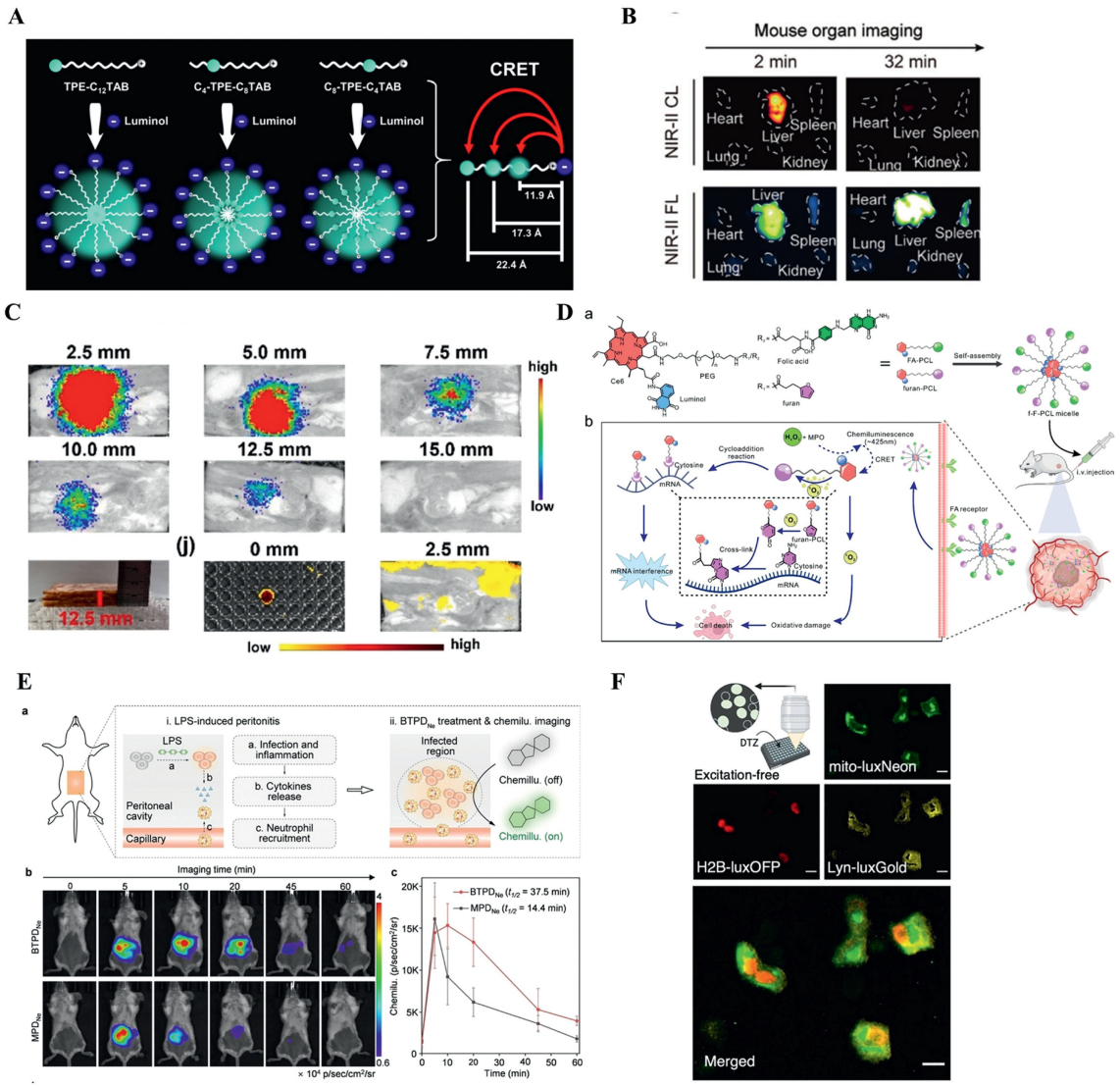


Fig. 4. (A) Scheme for synthesis of three types of AIE-active cationic micelles for investigating the quantitative correlation between CRET efficiency and donor-acceptor distance. Reproduced with permission [97]. Copyright 2021, Wiley-VCH GmbH. (B) Scheme of *ex vivo* NIR-II CL imaging and NIR-II FL imaging at 320mg/kg APAP dosage. Reproduced with permission [106]. Copyright 2025, Springer Nature. (C) Scheme of CL images of DTLum NPs in the presence of H_2O_2/NaClO mixture. Reproduced with permission [107]. Copyright 2025, Elsevier. (D) Schematic diagram of the synthesis of f-F-PCL micelle and furan for tumor SIPDT and mRNA interference. Reproduced with permission [108]. Copyright 2024, Wiley-VCH GmbH. (E) Schematic representation of neutrophil recruitment in LPS-triggered peritonitis and the detection process of $BTPD_{Ne}$. Reproduced with permission [109]. Copyright 2022, Wiley-VCH GmbH. (F) Scheme of excitation-free multiplexed luminescence image of subcellular structures. Reproduced with permission [106,117]. Copyright 2024, Elsevier.

Huang *et al.* designed a novel chemiluminescent agent based on benzoxazole-phenoxy-dioxetane [109]. By introducing intramolecular hydrogen bonding, the chemiluminescent half-life of this probe was extended by 33-fold, and its brightness increased by 8.2-fold, successfully enabling continuous dynamic imaging of neutrophils in mouse models of peritonitis and psoriasis for several hours (Fig. 4E). Additionally, traditional probe systems have lower costs, novel nanoprobes and high-end equipment still face cost bottlenecks. Miniaturization of semiconductor devices and the development of low-cost materials are expected to enhance cost-effectiveness, particularly demonstrating potential to replace traditional fluorescence technologies in grassroots medical and on-site detection applications.

2.4.2. Biologically induced fluorescence

BL, similar to CL, is another form of endogenously induced fluorescence that is not affected by external excitation light. It is typically achieved through enzymatic reactions within living organisms and is found in various species, including bacteria, fungi, insects, and marine life. As an emerging interdisciplinary technology, BL holds broad application prospects in modern science and technology. BL technology can be used for biological monitoring, ecological protection, biological detection, *in vivo* imaging, and gene expression research. Luciferin is a common material for bioluminescence-induced fluorescence [110]. Common luciferins include firefly luciferin and *Renilla* luciferin [111,112].

In addition, green fluorescent protein and its mutants are important fluorescent materials, but they suffer from limited bioluminescent colors, making simultaneous imaging of multiple targets difficult. Firefly luciferase is used for *in vivo* imaging but has low brightness, a large molecular weight, and relies on ATP/Mg^{2+} [113–115]. Furthermore, directed evolution based on natural templates struggles to meet the multiple criteria of ideal probes. The team of Hattori and Nagai proposed a strategy to expand bioluminescent color diversity through dual-receptor BRET [116]. By fusing fluorescent proteins (FPs) with NanoLuciferase (NLuc) to construct en-

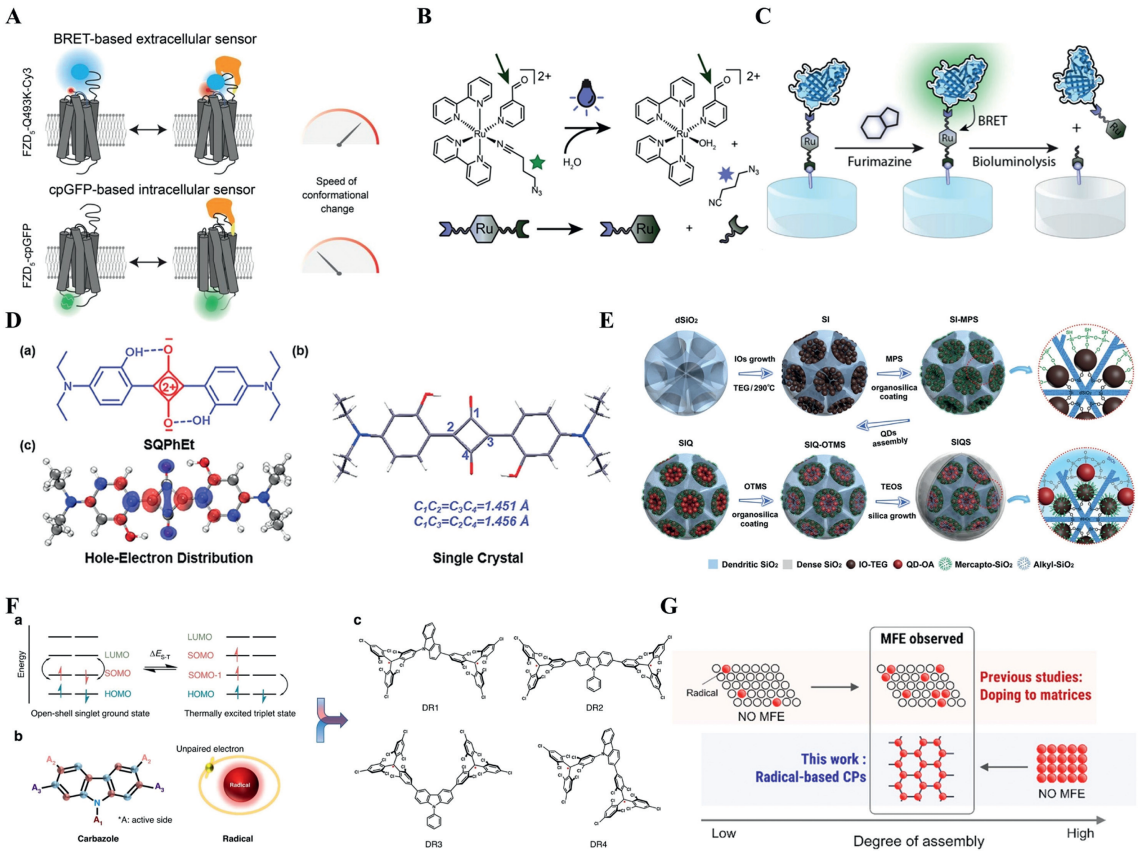


Fig. 5. (A) Scheme for kinetic analysis of WNT-induced conformational changes in FZD_5. Reproduced with permission [118]. Copyright 2021, The American Association for the Advancement of Science. (B) Scheme of photolysis of CHO-Ru-N_3. (C) Scheme for photocleavable linker for cargo release from polymer matrices *via* light or furimazine. Reproduced with permission [120]. Copyright 2021, Springer Nature. (D) Schematic illustration for the molecular formula, the single crystal structure and the hole-electron distributions of SQPhEt (isosurface value = 0.002). Reproduced with permission [131]. Copyright 2024, Wiley-VCH GmbH. (E) Schematic illustration for the synthetic route and structure of the SIQS nanosphere. Reproduced with permission [148]. Copyright 2021, Wiley-VCH GmbH. (F) Scheme for molecular design strategy: ground state configuration, carbazole bridge design, and structures of diradicals DR1–DR4. Reproduced with permission [151]. Copyright 2023, Springer Nature. (G) Schematic representation of comparison of magnetoluminescence approaches: doping in matrices and radical-based CP construction. Reproduced with permission [152]. Copyright 2021, American Chemical Society.

hanced nano-lantern variants, they successfully developed a series of 20-color bioluminescent proteins with significantly broadened spectral coverage by regulating energy transfer efficiency between NLuc and two FPs. Chen *et al.* developed entirely new luciferases through deep learning-driven protein design [117]. The second-generation neoLux series further achieves $a > 10$-fold brightness enhancement, combined with a compact size (13.7 kDa), high thermal stability (T_m > 100 °C), ATP independence, and high substrate specificity. By designing neoLux-FP fusion proteins, they expanded multicolor imaging capabilities *via* FRET (Fig. 4F).

And a myriad of FRET- and BRET-based biosensors have found applications in many fields, such as disease diagnosis, imaging *in vivo*, and detection of contaminants and pathogens. Using BRET-FRET technology, the work of Kowalski-Jahn *et al.* has designed a FZD-CRD biosensor (Fig. 5A) [118]. The sensor elucidates how the binding of WNT to FZD translates into receptor kinetics, and is also applicable to exploring the ligand-induced kinetics of other membrane receptors. Yan *et al.* used the BRET-FRET effect to activate myeloperoxidase (MPO)-dependent BL imaging *via* intravenous luminal injection to visualize tissue inflammation [119]. Rapp *et al.* [120] developed a heterobifunctional ruthenium cross-linker (CHO-Ru-N_3) that undergoes ligand exchange upon light exposure, enabling the release of biomolecules from hydrogel biomaterials (Fig. 5B). They demonstrated that protein release could be triggered either by direct illumination or BRET through conjugating the cross-linker to NLuc *via* sortase-tag enhanced protein ligation (STEPL) (Fig. 5C). This innovation allows for spatiotemporal control over protein release without the need for external light sources, addressing the limitations of light penetration in traditional PDT.

BRET technology shows expanding biomedical applications, particularly in PDT [121]. Bioluminescence-dependent enzyme-substrate reactions are sensitive to microenvironmental fluctuations and *in vivo* substrate distribution, with cellular redox changes reducing luciferase activity. Substrates may require multiple injections due to rapid metabolism, and novel substrates need toxicity evaluation. SNR is limited by fluorescent protein quantum yield and spectral overlap, causing crosstalk in multicolor imaging. Solutions include combining NanoLuc with NIR fluorescent proteins for reduced autofluorescence, using targeting peptide-modified upconversion nanoparticles (UCNPs) for tumor accumulation [122], and gene editing to regulate luciferase expression [123]. Engineering NanoLuc variants, screening high-efficiency NIR fluorescent proteins, and computational design of BRET pairs further enhance performance.

2.5. EL

EL refers to the photoelectric conversion where charge carriers inject into luminescent materials under an electric field, form excitons, and emit light [124]. It underlies modern optoelectronics, powering LED bulbs, automotive lights, and smartwatch screens [125]. Key electroluminescent materials include inorganic (GaN,

CdSe), organic (TADF), and perovskite materials [126–128], with recent advances in new materials and devices [129].

Luminescence efficiency in EL devices depends on injection efficiency, carrier balance, exciton utilization, and photon extraction [130]. Material modifications could boost efficiency. Tan *et al*. used ternary sensitization to suppress self-absorption in SQPhEt dye (Fig. 5D), achieving high PLQY [131]. In perovskite PeLEDs, Song *et al*. inserted PTLA to form a 3D heterojunction, confining carriers to solve efficiency roll-off [132]. The device showed 24.2 % EQE, 24,600 cd/m^2 luminance, and 127-h half-life at 100 cd/m^2. Current EL materials face numerous challenges, including biocompatibility issues, high costs, short lifespan, and difficulties in energy level matching [133–135].

In 2009, Adachi's team proposed TADF mechanism [136], converting triplet excitons to singlets *via* RISC in molecules with small singlet-triplet gaps, boosting IQE to 100 % [137,138]. A recent study by Yin *et al*. demonstrated a novel TADF-sensitized OLED that achieves 100 % exciton radiation depletion and reduces exciton annihilation on sub-microsecond timescales. This was achieved by designing sensitized host molecules with RISC and anti-aggregation properties, resulting in significant improvements in the device's EQE and power efficiency [139]. At the same time, compared to short-lived PFs in biological environments, which are difficult to distinguish from background signals in the nanosecond range, longer-lived DFs can be detected over a wider time scale, which is ideal for time-resolved imaging such as FLIM [140].

Although TADF materials theoretically enable 100 % exciton utilization without heavy metal doping, practical applications are constrained by challenges such as exciton quenching and spectral broadening from strong intermolecular π-π interactions at high doping, difficulty balancing spin-orbit coupling (SOC) and reverse intersystem crossing (RISC) efficiency, and increased ΔE_{ST} and decreased RISC due to conformational relaxation at high temperatures. Existing solutions such as introducing bulky groups or fluorination modification often lead to an increase in ΔE_{ST} or a decrease in SOC, making it difficult to balance narrow spectra, high exciton utilization efficiency, and thermal stability. To address exciton quenching-induced spectral broadening/efficiency loss in TADF materials at high doping, An *et al*. proposed a synergistic design strategy combining excited-state regulation and steric hindrance engineering [141]. The team constructed D-A type TADF molecules (5Cz-BNO and 5Cz-BN) using polycarbazole (5Cz) as donor units and rigid boron-nitrogen (B-N) acceptors. The steric effect of polycarbazole suppressed intermolecular π-π stacking, reducing exciton quenching at >10 wt% doping. This work overcame the bottleneck of simultaneously achieving "high doping-efficiency-narrow spectrum" in TADF materials, offering practical value for large-size OLED panels requiring high-doping processes.

During the high-performance development of OLED technology, in addition to the optimization of TADF materials in core properties such as exciton utilization efficiency, spectral stability, and thermal reliability, circularly polarized electroluminescence (CP-EL) has emerged as another frontier direction, attracting significant attention for its unique capability in polarized light modulation within display and photonics technologies. CP-EL is EL with circularly polarized light, with CPL divided into right ($\sigma+$) and left (σ-) handed types. This property in OLEDs holds promise for display and photonic tech, usually achieved by chiral luminescent materials or achiral material sensitization. But chiral structures cause problems. For example, they lead to exciton aggregation quenching when doping concentration of rigid chiral units exceeds 10 %, exciton recombination efficiency drops by over 30 % [142], and reverse intersystem crossing (RISC) efficiency falls from 100 % to under 60 %. Also, chiral structures disrupt molecular symmetry, increasing carrier injection barriers and mobility imbalances, which demands extra buffer layers, complicating device structures [143]. Jia *et al*. achieved CP OLEDs with high symmetry factor (1.1) and brightness (60,000 cd/m^2) using a chiral-free microcavity with 2D organic single crystals between silver layers [144]. Xu *et al*. proposed a "one-to-many" strategy sensitizing NUV CPL materials to enable CP-EL, yielding high PL quantum yields and CPL asymmetry factors for blue-to-red CP-PL in fluorescent, phosphorescent, TADF, and multi-resonance TADF systems. As OLED emissive layers, they achieve 9.0 % external quantum efficiency at 404 nm with minimal roll-off, leveraging triplet-singlet conversion in achiral TADF layers [145]. Future research should integrate computational chemistry and TADF exciton management to address sensitizer synthesis bottlenecks and spectral matching limitations.

In summary, EL currently covers a wide range of applications from daily lighting to high-end displays and biomedicine through the high efficiency and stability of inorganic semiconductors and the flexible tunability of organic molecules. However, the development of new high-performance materials is still in its infancy, facing multiple bottlenecks such as the difficulty in balancing efficiency and stability. For example, blue TADF materials suffer from a lifetime of <500 h due to exciton-exciton annihilation, and perovskite materials exhibit poor humidity and thermal stability, and challenges in precise regulation of spectral purity and color coordinates, failing to meet display standards for color coordinates and high doping causing spectral broadening. The future will advance toward the development of new luminescent materials that are efficient, stable, and environmentally friendly.

2.6. Magnetoluminescence

Magnetoluminescence refers to the change in material luminescent properties (*e.g.*, intensity, wavelength) under a magnetic field [146]. Magnetofluorescent materials (rare-earth doped, QDs, magnetic nanomaterials) show potential in spintronics and biomedical imaging [147]. Huang *et al*. developed SIQS (Fig. 5E) by integrating iron oxide NPs and QDs in silica templates, enabling PCT detection in serum [148]. Molaei *et al*. designed Fe_3O_4@SiO_2@alginate nanohybrids with CQDs for pH-responsive drug delivery [149]. The nanohybrids show 81 % drug loading, releasing 25 % (pH 7.4) and 38 % (pH 5.5) of drugs within 48 h, with enhanced release in simulated tumor environments, indicating potential for combined drug delivery and bioimaging.

However, magnetoluminescent materials suffer from matrix dependence and low efficiency. The balance of spin configurations and exciton behavior in such materials is highly dependent on the matrix environment, as the matrix must regulate the exchange interactions between radicals to achieve magnetic field responsiveness. Improper assembly, however, can lead to strong coupling or non-radiative quenching. Additionally, low spin-orbit coupling efficiency, aggregation-caused quenching (ACQ), and energy competition between the matrix and radicals collectively result in insufficient luminescence efficiency. To develop more materials suitable for magnetofluorescence, researchers have made additional efforts.

Open-shell singlet biradicals possess unique optical, electrical, and magnetic properties, but still face challenges of matrix dependence and efficiency [150]. Open-shell biradicals offer solutions. Abdurahman's team developed DR1 (Fig. 5F), a biradical with 210 % magnetoluminescence under 7 T [151]. Matsuoka observed single-molecule magnetoluminescence in radical dimers [146], while Kimura achieved magnetoluminescence in CPs with "moderate radical assembly" (Fig. 5G), where bisZn CPs switch between non-luminescence and luminescence under fields [152]. Studies on molecular design and mechanism exploration of radical systems in magnetoluminescence have revealed the critical roles of spin regulation and assembly strategies in determining luminescence efficiency and magnetic responsiveness. Building on these

insights, researchers have further applied magnetoluminescence to practical applications in biomedicine.

Exosomes are small membrane-bound vesicles released by cells, encapsulating a variety of macromolecules including nucleic acids, proteins, and lipids. These vesicles are ubiquitous in diverse bodily fluids and primarily function in facilitating communication between cells [153]. And the exosomes that carry distinct membrane proteins are emerging as novel biomarkers for liquid biopsies. Luo *et al.* introduced an integrated magnetofluorescent nanosensor (iMFEX) for rapid and sensitive detection of tumor-derived exosomes [154]. Aiming at the challenge of low surface protein content in exosomes, the researchers designed a new platform: magnetic nanoparticles (MB@DTLP) were used for efficient exosome capture, a bifunctional aptamer (PD-L1-T) specifically recognized the exosomal membrane protein programmed death-ligand 1 (PD-L1), and initiated catalytic hairpin assembly (CHA). CHA generated H1/H2 duplexes containing PAM sequences, activating the trans-cleavage activity of Cas12a protein to amplify fluorescence signals. The iMFEX nanosensor showed high specificity and sensitivity for detecting tumor-derived PD-L1-positive exosomes, with a linear range of 2.86×10^3–2.86×10^7 particles/μL and a detection limit of 1.71×10^3 particles/μL. It effectively distinguished non-small cell lung cancer patients from healthy individuals, with an area under the curve (AUC) of 0.89, 80 % sensitivity, and 90 % specificity in receiver operating characteristic (ROC) curve analysis, outperforming traditional enzyme-linked immunosorbent assay (ELISA) methods. This study first integrates aptamer-mediated signaling with CHA-CRISPR/Cas12a cascade signaling for exosome analysis in a single sensing system.

Although much materials exhibit magnetoluminescent properties at low temperatures, their application at room temperature is limited. Thermal fluctuations cause the Zeeman splitting to decrease as temperature rises, necessitating a low-temperature environment for practical applications, which increases the complexity and cost of the device. However, Chen *et al.* recently reported room-temperature intrinsic magnetically CP-PL in 2D Er_2O_2S sheets, a discovery that holds new promise in the field of magnetoluminescence (Fig. 6A) [155]. The geff factor of 2D Er_2O_2S is maintained at about −6.3 from the temperature limit of liquid helium to room temperature and remains independent of temperature. This phenomenon is different from previous materials where the Seeman splitting decreases with increasing temperature due to thermal fluctuations. The anomalous temperature-dependent magnetically induced CP-PL in 2D Er_2O_2S is confirmed by temperature-dependent Raman spectroscopy and theoretical calculations to originate from the weak electron-phonon coupling. This study provides a new direction for optimizing material properties and exploring new magnetoluminescence mechanisms.

3. Cross-applications, challenges and prospects

Each imaging modality possesses distinct advantages and limitations (Table S1 in Supporting information). PL features mature technology and multicolor imaging. ML enables real-time mechanical signal detection for smart devices. Ultrasound-induced luminescence offers high penetration and resolution, while X-ray-induced luminescence allows rapid non-destructive analysis. Cherenkov luminescence pairs widely with PET/SPECT. CL provides fast imaging with high SNR, and BL shows excellent biocompatibility. EL achieves efficient energy conversion in optoelectronic devices. Magnetoluminescence allows magnetic field control, though less studied, its specificity offers irreplaceable applications. When single excitation modes are insufficient, combining multiple modes integrates their strengths, compensating for individual limitations. This synergistic approach enables high sensitivity, deep penetration, high resolution, and real-time dynamic detection, driving cross-disciplinary advances in life sciences, materials engineering, and environmental monitoring.

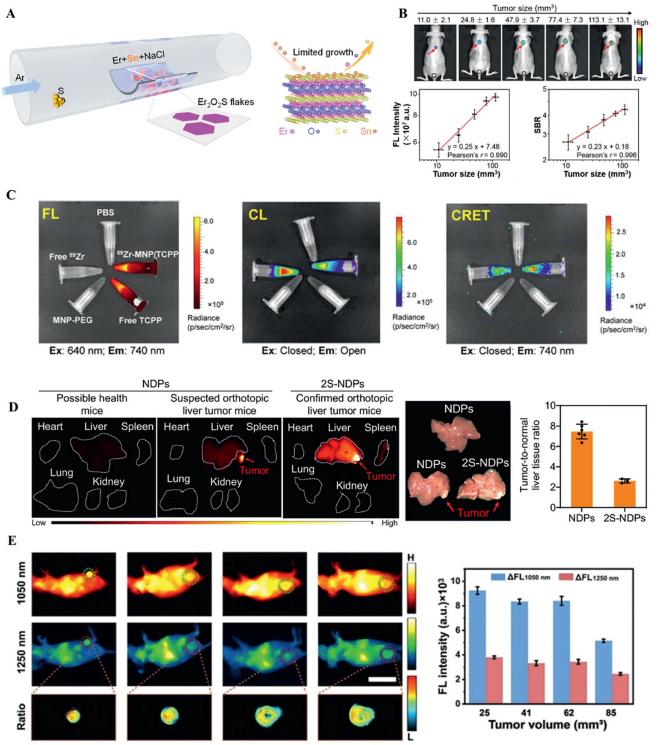


Fig. 6. (A) Schematic illustration for synthesis, growth mechanism, characterization, and DFT-calculation of 2D Er_2O_2S. Reproduced with permission [155]. Copyright 2024, American Chemical Society. (B) Scheme to illustrate NIR fluorescence images of HeLa tumors of different sizes in mice treated with P-Cy-TCO&Bio + SA. Reproduced with permission [156]. Copyright 2024, American Chemical Society. (C) Scheme for the FL, CL and CRET images of different solution samples. Reproduced with permission [157]. Copyright 2018, American Chemical Society. (D) Scheme for representative *in vitro* NIR-II fluorescence images of NDPs treated with 2S-NDPs. Reproduced with permission [158]. Copyright 2025, Springer Nature. (E) Scheme for NIR-II FL and NIR-II FL ratio plots of mice after 24 h of radiotherapy; corresponding FL intensity to tumor ratios. Reproduced with permission [160]. Copyright 2023, Wiley-VCH GmbH.

Moreover, the probes combined with different energy sources show excellent multimodal properties in complex biological systems, providing more comprehensive information support for comprehensive disease diagnosis.

Combining MRI and NIR-FL enables simultaneous anatomical and molecular imaging. Weng *et al.* proposed an orthogonal dual pre-targeting strategy using P-Cy-TCO&Bio probe, which self-assembles into nanoparticles to capture Gd-chelate and IR780 for enhanced NIR-FL (Fig. 6B)/MRI contrast [156]. Ni *et al.* developed ^{89}Zr-MNP/TCPP with porphyrin modification, accumulating in tumors under magnetic field for CRET multimodal imaging and improved CRIT (Fig. 6C) [157].

NIR-II imaging overcomes NIR-I limitations. Yang's NDP probe activates NIR-II fluorescence in liver tumors (Fig. 6D), enabling 100 % accurate detection of ≥4 mm lesions [158]. Xiao *et al.*'s first NIR-II FL/PA bimodal ratiometric probe (RAPNP) enables NO detection but struggles with *in-situ* dynamic monitoring of endogenous NO due to irreversible binding mechanisms [159]. Nevertheless, the *in situ* and dynamic real-time monitoring of endogenous NO remains elusive, largely due to the irreversible binding mechanisms inherent in most existing NO probes. Ge's BBT-IR/Se-MN probe targets ROS, while Hu's NIR-II-H_2S_2 probe quantifies H_2S_2 with 1.8 nmol/L limit for liver injury monitoring (Fig. 6E) [160,161]. Current challenges include organ-specific targeting and balancing FL/PA signal intensities.

Multimodal imaging combines multiple techniques to integrate anatomical, functional, and molecular information for enhanced diagnostic accuracy, enabling deep tissue imaging and multi-target analysis. However, challenges remain, including complex multi-energy-source co-excitation design, the need for efficient energy conversion and signal enhancement, the biocompatibility and safety of probes, energy transfer loss in biological systems, and the development of low-cost multifunctional devices. Combining cancer therapies overcomes limitations of traditional approaches like chemotherapy's non-specific toxicity [162] and PDT's reliance on light/oxygen. Future advancements will optimize multi-energy-source fluorescence excitation *via* intelligent probes, integrate optical/electrical/magnetic/acoustic modes in multimodal imaging, and improve NIR-II probes for deeper penetration. Leveraging AI for data analysis will enhance signal recognition and quantitative efficiency, driving progress in biomedical diagnostics, disease typing, and functional material development.

4. Conclusion

Advancements in imaging technology and extensive research have led to innovative strategies based on fluorescence excitation from various energy sources. By exploring and utilizing diverse energy strategies, including light energy, mechanical energy, EMR, chemical energy, bioenergy, electrical energy, and magnetic energy, researchers have developed a wide range of fluorescence excitation systems. These innovations have greatly expanded the applications of fluorescence technology in fields such as biomedicine, materials science and environmental monitoring. Two-photon fluorescence has demonstrated notable advantages for deep tissue imaging, including low phototoxicity and high resolution. Ultrasound-induced fluorescence is emerging as a promising approach for tumor diagnosis and treatment due to its excellent biosafety and cost-effectiveness. X-ray and Cerenkov radiation-induced fluorescence systems offer high penetration capabilities and sensitivity. Additionally, magnetoluminescence presents a new perspective for targeted imaging and drug delivery. EL has demonstrated significant value in electrochemical analysis and biosensing. CRET and BRET have great contributions in eliminating background fluorescence.

Nevertheless, there are still many challenges in different energy source excitation strategies. For example, how to improve the energy conversion efficiency to optimize the signal output, how to design highly sensitive and selective probes to adapt to complex biological environments, and how to achieve efficient synergy of multiple energy sources to cope with more complex application scenarios are still key scientific issues for future development. The integration and intelligent development of multi-energy-source strategies are also urgent breakthroughs in this field.

In the future, the integration of emerging fields such as nanomaterials science, molecular design technology, and artificial intelligence is anticipated to drive significant advancements in fluorescence excitation strategies based on diverse energy sources. This convergence is expected to lead to enhanced performance and broader application potential across various domains. For example, the development of composite probes with multifunctionality and high biocompatibility can realize the integration of imaging and therapy; the introduction of multimodal synergistic imaging technology combining photoacoustic (PA), magnetic resonance, and fluorescence imaging will provide more comprehensive and accurate diagnostic information; the use of deep learning algorithms to process complex imaging data will significantly improve the efficiency and accuracy of signal analysis. In conclusion, the continuous innovation and integration of fluorescence strategies induced by different energy sources will promote the wide application of fluorescence technology in scientific research and practical applications, opening up more possibilities for biomedical diagnosis, environmental protection and new material development.

This review summarizes a wide range of modes that have been used in recent years for fluorescence molecular imaging in biomedical and materials science based on the classification of excitation energy sources, such as lasers, X-rays, nuclides, chemical energy, bioenergy, electrical energy and magnetic energy. The continuous emergence of emerging excitation modalities not only promotes the rapid development of biomedical diagnostic technology, but also opens up new directions for the future of translational medicine. Despite numerous challenges in the practical application of various excitation strategies, these innovative fluorescence excitation concepts and their evolving biomedical applications offer significant inspiration for interdisciplinary researchers, fostering further innovation and exploration in related fields. The combination of fluorescence excitation strategies through the synergistic action of different energy sources provides new ideas for achieving more efficient, sensitive and versatile imaging and sensing. Future developments will focus on the design of novel composite probes to further enhance biocompatibility, signal strength and multimodal imaging capabilities, which will lead to deeper advances in the fields of biomedicine, environmental science and materials engineering.

Declaration of competing interest

The authors declare that they have no known competing financial interests or personal relationships that could have appeared to influence the work reported in this paper.

CRediT authorship contribution statement

Jingwen Zheng: Writing – original draft, Project administration. **Yubo Tan:** Writing – original draft, Project administration. **Dazhuang Xu:** Writing – original draft, Funding acquisition. **Gang Liu:** Writing – review & editing, Funding acquisition. **Zhixiang Lu:** Writing – review & editing, Project administration, Funding acquisition.

Acknowledgments

This work was supported by the National Key Research and Development Program of China (Nos. 2023YFC2415700, 2023YFB3810000), the National Natural Science Foundation of China (NSFC, Nos. 82402426, U22A20333), the Natural Science Foundation of Sichuan Province (No. 2024NSFSC1741), the Fundamental Research Funds for the Central Universities (No. 20720240051), Xiang'an Innovation Laboratory Science and Technology Project (No. 2024XAKJ0102008) and the Postdoctoral Fellowship Program of CPSF (No. GZC20231400).

Supplementary materials

Supplementary material associated with this article can be found, in the online version, at doi:10.1016/j.cclet.2025.111552.

References

[1] E. Wiedemann, Ann. Phys. 270 (1888) 446–463.
[2] B. Valeur, M.N. Berberan-Santos, Molecular Fluorescence: Principles and Applications, 2nd, John Wiley & Sons, Weinheim, 2013.
[3] A. Trivelli, Sci. Mon. 33 (1931) 175–179.
[4] A.J. Wollman, R. Nudd, E.G. Hedlund, M.C. Leake, Open Biol. 5 (2015) 150019.
[5] M. Titford, Biotech. Histochem. 80 (2005) 73–78.
[6] Immunohistochemistry in historical perspective: Knowing the past to understand the present C.O. Hidalgo, Immunohistochemistry and Immunocytochemistry: Methods and Protocols Springer, New York, 2021, pp. 17–31.
[7] L.A. Herzenberg, D. Parks, B. Sahaf, O. Perez, M. Roederer, L.A. Herzenberg, Clin. Chem. 48 (2002) 1819–1827.

[8] S. Dunst, P. Tomancak, Genetics 211 (2019) 15–34.
[9] M. Yuan, X. Fang, W. Liu, et al., ACS Appl. Bio Mater. 8 (2024) 368–373.
[10] R. Cesareo, G. Viezzoli, Phys. Med. Biol. 28 (1983) 1209–1218.
[11] R. Terzano, M.A. Denecke, G. Falkenberg, B. Miller, D. Paterson, K. Janssens, Phys. Med. Biol. 91 (2019) 1029–1063.
[12] R.H. Tykot, Appl. Spectrosc. 70 (2016) 42–56.
[13] S. Bedouhène, F. Moulti-Mati, M. Hurtado-Nedelec, P.M.C. Dang, J. El-Benna, Am. J. Blood Res. 7 (2017) 41–48.
[14] R. Singh, Crit. Rev. Anal. Chem. 52 (2022) 35–52.
[15] R.H. Friend, R. Gymer, A. Holmes, et al., Nature 397 (1999) 121–128.
[16] M.C. Tang, M.Y. Chan, V.W.W. Yam, Chem. Rev. 121 (2021) 7249–7279.
[17] Z. Cui, A. Abdurahman, X. Ai, F. Li, CCS Chem. 2 (2020) 1129–1145.
[18] S. Gao, Z. Cui, F. Li, Chem. Soc. Rev. 52 (2023) 2875–2885.
[19] J.R. McCarthy, R. Weissleder, Adv. Drug Del. Rev. 60 (2008) 1241–1251.
[20] Y. Luo, K. Zhang, Z. Ding, et al., Nat. Commun. 13 (2022) 6892.
[21] Y. Takubo, Rev. Laser Eng. 11 (1983) 287–295.
[22] M. Lelek, M.T. Gyparaki, G. Beliu, et al., Nat. Rev. Methods Primers 1 (2021) 39.
[23] D.N. Hanlon, I. Todd, E. Peekstok, W.M. Rainforth, S. van der Zwaag, Wear 251 (2001) 1159–1168.
[24] W. Denk, J.H. Strickler, W.W. Webb, Science 248 (1990) 73–76.
[25] M.J. Rust, M. Bates, X. Zhuang, Nat. Methods 3 (2006) 793–796.
[26] F. Wang, F. Ren, Z. Ma, et al., Nat. Nanotechnol. 17 (2022) 653–660.
[27] J. Teixeira, T. Lopes, D. Capela, et al., Sci. Rep. 15 (2025) 3515.
[28] M.J. Serafino, J.A. Jo, Biomed. Opt. Express. 14 (2023) 1608–1625.
[29] C.W. Chang, D. Sud, M.A. Mycek, Methods Cell Biol. 81 (2007) 495–524.
[30] E. Perego, S. Zappone, F. Castagnetti, et al., Nat. Commun. 14 (2023) 8224.
[31] Z.X. Liang, Y.Y. Zhao, J.T. Chen, et al., Nat. Commun. 16 (2025) 2086.
[32] L. Zeng, X.Y. Wang, N. Li, J. Pang, X.H. Bu, Coord. Chem. Rev. 511 (2024) 215868.
[33] L. Wu, J. Liu, P. Li, B. Tang, T.D. James, Chem. Soc. Rev. 50 (2021) 702–734.
[34] D. Wang, G. Wang, K. Liu, et al., Chin. Chem. Lett. 33 (2022) 2532–2536.
[35] T. Jiang, D. Li, Y. Hang, et al., Dyes Pigm. 133 (2016) 201–213.
[36] Y.R. Meng, M.J. Xu, S.F. Li, et al., Inorg. Chem. 63 (2024) 17856–17863.
[37] F. Brandl, S. Bergwinkl, C. Allacher, B. Dick, Chem. Eur. J. 26 (2020) 7946–7954.
[38] B.K.K. Pragti, R. Chen, J. Diao, Y. Sun, Adv. Healthc. Mater. 14 (2025) 2403272.
[39] J. Zhang, Y. Tang, Q. Duan, et al., J. Lumin. 277 (2025) 120921.
[40] Y.J. Fu, S.S. Shen, X.F. Guo, H. Wang, J. Mater. Chem. B 8 (2020) 1422–1431.
[41] R. Chen, K. Qiu, D.C.Y. Leong, et al., Biosens. Bioelectron. 239 (2023) 115604.
[42] T.H. Chia, A. Williamson, D.D. Spencer, M.J. Levene, Opt. Express. 16 (2008) 4237–4249.
[43] Y. Guo, Z. Huang, L. Wang, et al., Anal. Chem. 97 (2025) 5744–5752.
[44] N. Bondon, C. Charlot, L.M. Ali, et al., J. Mater. Chem. B 13 (2025) 1767–1780.
[45] P. Wang, C. Chen, H. Ren, E. Duan, Chin. Chem. Lett. 36 (2025) 110725.
[46] P. Gao, Z. Xie, M. Zheng, Chin. Chem. Lett. 33 (2022) 1659–1672.
[47] D. Chen, X. Guo, X. Sun, et al., Exploration 4 (2024) 20230166.
[48] Y. Guo, Z. Li, B. Guo, B. Wang, Y. Tu, Nano Biomed. Eng. 16 (2024) 135–151.
[49] F. Li, Y. Lai, J. Ye, et al., Acta Pharm. Sin. B 12 (2022) 3486–3497.
[50] T. Li, Y. Zhang, F. Wu, et al., Small Methods 9 (2025) 2400132.
[51] J. Sun, W. Cai, Y. Sun, C. Guo, R. Zhang, Int. J. Nanomed. 15 (2020) 10199–10213.
[52] Y. Li, D. Hu, Z. Sheng, et al., Biomaterials 264 (2021) 120365.
[53] Y. Yang, Y. Xie, F. Zhang, Adv. Drug Del. Rev. 193 (2023) 114697.
[54] W. Pan, M. Rafiq, W. Haider, et al., Coord. Chem. Rev. 514 (2024) 215907.
[55] J. Wang, K. Yao, K. Cui, et al., Adv. Opt. Mater. 11 (2023) 2203112.
[56] F. Wang, P. Lv, S. Yang, et al., Laser Photonics Rev. 19 (2025) 2401971.
[57] H.U. Rahim, M. Qaswar, M. Wang, X. Jing, X. Cai, J. Environ. Chem. Eng. 9 (2021) 106696.
[58] L. Wang, Z. Shang, M. Shi, et al., RSC Adv. 10 (2020) 11418–11425.
[59] P. Gao, J. Wang, J. Wu, et al., Coatings 13 (2023) 808.
[60] Z. Xie, H. Deng, X. Ge, Z. Chi, B. Liu, J. Am. Chem. Soc. 147 (2025) 12722–12729.
[61] S.J. Doktycz, K.S. Suslick, Science 247 (1990) 1067–1069.
[62] S. Liang, D. Hu, G. Li, et al., Sci. Bull. 67 (2022) 2316–2326.
[63] Y. Wang, Y. Yu, X. Wei, F. Narita, Adv. Mater. Technol. 7 (2022) 2200318.
[64] Q. Zhou, S. Lau, D. Wu, K.K. Shung, Prog. Mater. Sci. 56 (2011) 139–174.
[65] A. Sridharan, J.R. Eisenbrey, F. Forsberg, et al., Pediatr Radiol. 51 (2021) 2117–2127.
[66] A. Valimukhametova, O. Zub, N. Castro-Lopez, et al., ACS Appl. Bio Mater. 8 (2025) 4303–4314.
[67] Y. Pu, B. Zhou, J. Bing, et al., Nat. Commun. 15 (2024) 9023.
[68] Y. Wang, Z. Yi, J. Guo, et al., Nat. Photon. 18 (2024) 334–343.
[69] C. Xu, J. Huang, Y. Jiang, et al., Nat. Biomed. Eng. 7 (2023) 298–312.
[70] Y. Zhong, X. Yu, W. Li, J. Mater. Chem. C 13 (2025) 1036–1062.
[71] A. Galli, L. Bonizzoni, Appl. Sci. 12 (2022) 6309.
[72] A. Frydrych, K. Jurowski, TrAC Trends Anal. Chem. 166 (2023) 117165.
[73] M. Strotton, T. Hosogane, M. di Michiel, et al., Nat. Methods 20 (2023) 1310–1322.
[74] Y. Song, H. Zhao, Y. Zi, et al., ACS Energy Lett. 8 (2023) 2232–2240.
[75] Z. Jia, Y. Li, R. Li, et al., J. Alloys Compd. 960 (2023) 170825.
[76] J. Huang, L. Su, C. Xu, et al., Nat. Mater. 22 (2023) 1421–1429.
[77] N. Zhang, R. Zhang, X. Xu, et al., Adv. Opt. Mater. 11 (2023) 2300187.
[78] P. Pei, Y. Chen, C. Sun, et al., Nat. Nanotechnol. 16 (2021) 1011–1018.
[79] H. Chen, X. Sun, G.D. Wang, et al., Mater. Horiz. 4 (2017) 1092–1101.
[80] X. Wang, L. Li, J. Li, et al., Photonics 9 (2022) 390.
[81] Z. Yang, T.T. Pang, Z.J. Wu, et al., EJNMMI Res. 15 (2025) 33.
[82] N. Kotagiri, G.P. Sudlow, W.J. Akers, S. Achilefu, Nat. Nanotechnol. 10 (2015) 370–379.
[83] D. Duan, H. Liu, Y. Xu, et al., ACS Appl. Mater. Interfaces 10 (2018) 5278–5286.
[84] J. Li, S. Dai, R. Qin, et al., ACS Appl. Mater. Interfaces 13 (2021) 54727–54738.
[85] Q. Wu, Y. Zhang, G. Jia, et al., Nano Today 52 (2023) 101984.
[86] B.E. Mc Larney, Q. Zhang, E.C. Pratt, et al., J. Nucl. Med. 64 (2023) 177–182.
[87] Y.A. Chen, J.J. Li, S.L. Lin, et al., Int. J. Mol. Sci. 22 (2021) 4934.
[88] Q. Zhang, E.C. Pratt, R. Tamura, et al., Nano Lett. 21 (2021) 4217–4224.
[89] T.M. Shaffer, E.C. Pratt, J. Grimm, Nat. Nanotechnol. 12 (2017) 106–117.
[90] N. Liu, X. Su, X. Sun, Theranostics 12 (2022) 7404.
[91] J. Li, Y. Li, J. Ming, et al., Angew. Chem. Int. Ed. 63 (2024) e202401683.
[92] J. Hu, B. Zhao, R. Wen, et al., Nano Lett. 23 (2023) 5209–5216.
[93] Z.T. Rosenkrans, J.C. Hsu, E. Aluicio-Sarduy, et al., Adv. Funct. Mater. 33 (2023) 2302777.
[94] Y. Wu, T. Jiang, Micromachines 13 (2022) 1789.
[95] H. Sahoo, J. Photochem. Photobiol. C: Photochem. Rev. 12 (2011) 20–30.
[96] Y. Yan, X.y. Wang, X. Hai, et al., TrAC Trends Anal. Chem. 123 (2020) 115755.
[97] J. Lou, X. Tang, H. Zhang, W. Guan, C. Lu, Angew. Chem. Int. Ed. 60 (2021) 13029–13034.
[98] F. Barni, S.W. Lewis, A. Berti, G.M. Miskelly, G. Lago, Talanta 72 (2007) 896–913.
[99] M.A. Moroz, J. Zurita, A. Moroz, et al., Mol. Ther. Oncolytics 21 (2021) 15–22.
[100] Y. Yan, P. Shi, W. Song, S. Bi, Theranostics 9 (2019) 4047.
[101] M. Yang, J. Huang, J. Fan, et al., Chem. Soc. Rev. 49 (2020) 6800–6815.
[102] P. Khan, D. Idrees, M.A. Moxley, et al., Appl. Biochem. Biotechnol. 173 (2014) 333–355.
[103] M.A. Tzani, D.K. Gioftsidou, M.G. Kallitsakis, et al., Molecules 26 (2021) 7664.
[104] H.W. Yeh, H.W. Ai, Annu.l Rev. Anal. Chem. 12 (2019) 129–150.
[105] L. Li, T. Hu, J. Guo, J. Zhang, Adv. Sensor Res. 2 (2023) 2200103.
[106] Z. Chen, Q. Li, Y. Wu, J. Liu, L. Liu, L. Su, R. Wu, J. Song, Nat. Commun. 16 (2025) 238.
[107] J. Li, S. Bian, T. Liu, et al., Biosens. Bioelectron. 270 (2025) 116978.
[108] Y. Li, X.L. Lei, X.S. Zhang, et al., Angew. Chem. 136 (2024) e202411598.
[109] J. Huang, P. Cheng, C. Xu, et al., Angew. Chem. Int. Ed. 61 (2022) e202203235.
[110] S.M. Marques, J.C.G. Esteves da Silva, IUBMB Life 61 (2009) 6–17.
[111] S.H.D. Haddock, M.A. Moline, J.F. Case, Annu. Rev. Mar. Sci. 2 (2010) 443–493.
[112] E. Brodl, A. Winkler, P. Macheroux, Comput. Struct. Biotechnol. J. 16 (2018) 551–564.
[113] B.R. Branchini, T.L. Southworth, N.F. Khattak, E. Michelini, A. Roda, Anal. Biochem. 345 (2005) 140–148.
[114] B.A. Tannous, D.E. Kim, J.L. Fernandez, R. Weissleder, X.O. Breakefield, Mol. Ther. 11 (2005) 435–443.
[115] A.M. Loening, T.D. Fenn, A.M. Wu, S.S. Gambhir, Protein Eng. Desi. Select. 19 (2006) 391–400.
[116] M. Hattori, T. Wazawa, M. Orioka, Y. Hiruta, T. Nagai, Sci. Adv. 11 (2025) eadp4750.
[117] J.Y.H. Chen, Q. Shi, X. Peng, et al., Chem 11 (2025) 102346.
[118] M. Kowalski-Jahn, H. Schihada, A. Turku, et al., Sci. Adv. 7 (2021) eabj7917.
[119] X. Yan, C. Yang, M. Yang, et al., J. Nanobiotechnol. 20 (2022) 99.
[120] T.L. Rapp, I. Kopyeva, A. Adhikari, C.A. DeForest, J. Am. Chem. Soc. 146 (2024) 25397–25402.
[121] D.O. Borroto-Escuela, M. Flajolet, L.F. Agnati, P. Greengard, K. Fuxe, Methods Cell Biol. 117 (2013) 141–164.
[122] O. Shapoval, V. Patsula, D. Větvička, et al., Biomacromolecules 25 (2024) 5771–5785.
[123] M.K. Schwinn, T. Machleidt, K. Zimmerman, et al., ACS Chem. Biol. 13 (2018) 467–474.
[124] S. Kumar, J. Jagielski, T. Marcato, S.F. Solari, C.J. Shih, J. Phys. Chem. Lett. 10 (2019) 7560–7567.
[125] Y. Dong, H. Chen, J. He, S.T. Wu, Inf. Display 33 (2017) 6–14.
[126] Q. Fu, Z. Hu, M. Zhou, J. Lu, Z. Ni, Laser Photonics Rev. 15 (2021) 2000587.
[127] S.V. Rangnekar, V.K. Sangwan, M. Jin, M. Khalaj, et al., ACS Nano 17 (2023) 17516–17526.
[128] S. Rhee, J.H. Chang, D. Hahm, et al., ACS Nano 14 (2020) 17496–17504.
[129] D. Guo, X. Le, H. Shang, et al., Chin. Chem. Lett. 34 (2023) 108347.
[130] J. Lin, Q. Sun, W. Feng, et al., Adv. Photon. Res. 2 (2021) 2000145.
[131] W. Tan, Y. Yu, T. Shi, et al., Adv. Mater. 36 (2024) 2410418.
[132] Y.H. Song, B. Li, Z.J. Wang, et al., Nature 641 (2025) 352–357.
[133] Y. Xu, Y. Lv, R. Wu, et al., Inorg. Chem. 60 (2021) 6503–6513.
[134] S.K. Lee, E.J. McLaurin, Curr. Opin. Green Sust. Chem. 12 (2018) 76–82.
[135] D. Wang, C. Cheng, T. Tsuboi, Q. Zhang, CCS Chem. 2 (2020) 1278–1296.
[136] A. Endo, M. Ogasawara, A. Takahashi, et al., Adv. Mater. 21 (2009) 4802–4806.
[137] Y. Tao, K. Yuan, T. Chen, et al., Adv. Mater. 26 (2014) 7931–7958.
[138] C. Adachi, Jpn. J. Appl. Phys. 53 (2014) 060101.
[139] C. Yin, Y. Xin, T. Huang, et al., Nat. Commun. 16 (2025) 30.
[140] C. Yin, Y. Zhang, T. Huang, et al., Sci. Adv. 8 (2022) eabp9203.
[141] R.Z. An, F.M. Zhao, C. Shang, M. Zhou, L.S. Cui, Angew. Chem. Int. Ed. 64 (2025) e202420489.
[142] I.E. Serdiuk, M. Mońka, K. Kozakiewicz, et al., J. Phys. Chem. B 125 (2021) 2696–2706.
[143] O. García Mancheño, M. Waser, Eur. J. Org. Chem. 26 (2023) e202200950.
[144] J. Jia, X. Cao, X. Ma, et al., Nat. Commun. 14 (2023) 31.
[145] L. Xu, H. Liu, X. Peng, et al., Angew. Chem. Int. Ed. 62 (2023) e202300492.
[146] R. Matsuoka, S. Kimura, T. Miura, T. Ikoma, T. Kusamoto, J. Am. Chem. Soc. 145 (2023) 13615–13622.

[147] A. Matiushkina, A. Bazhenova, I. Litvinov, et al., J. Phys. Conf. Ser. 1866 (2021) 012003.
[148] L. Huang, Y. Zhang, T. Liao, et al., Small 17 (2021) 2100862.
[149] M.J. Molaei, E. Salimi, Mater. Chem. Phys. 288 (2022) 126361.
[150] Y. Zhu, Z. Zhu, S. Wang, Q. Peng, A. Abdurahman, Angew. Chem. Int. Ed. 64 (2025) e202423470.
[151] A. Abdurahman, L. Shen, J. Wang, et al., Light Sci. Appl. 12 (2023) 272.
[152] S. Kimura, R. Matsuoka, S. Kimura, H. Nishihara, T. Kusamoto, J. Am. Chem. Soc. 143 (2021) 5610–5615.
[153] A. Mohseni, F. Salehi, S. Rostami, et al., Stem Cell Res. 16 (2025) 6.
[154] S. Luo, Y. Wu, W. Pan, et al., Sensors Actuators B: Chem. 374 (2023) 132792.
[155] P. Chen, B. Peng, Z. Liu, et al., J. Am. Chem. Soc. 146 (2024) 6053–6060.
[156] J. Weng, Z. Huang, Y. Liu, et al., J. Am. Chem. Soc. 146 (2024) 13163–13175.
[157] D. Ni, C.A. Ferreira, T.E. Barnhart, et al., J. Am. Chem. Soc. 140 (2018) 14971–14979.
[158] Y. Tang, Y. Li, C. He, et al., Nat. Commun. 16 (2025) 278.
[159] P. Xiao, M. Liang, S. Yang, et al., Biomaterials 294 (2023) 121993.
[160] X. Ge, L. Su, Z. Chen, et al., Angew. Chem. 135 (2023) e202305744.
[161] B. Hu, Q. Liu, Y. Jiang, et al., Angew. Chem. Int. Ed. 64 (2025) e202418378.
[162] D.N. Yadav, D. Harijan, S.V. Pogu, G. Prabusankar, A.K. Rengan, Med. Comm. Biomater. Appl. 4 (2025) e70004.